Voltage Readjustment Methodology According to Pressure and Temperature Applied to a High Temperature PEM Fuel Cell

Mathieu Baudy, Olivier Rondeau, Amine Jaafar, Christophe Turpin, Sofyane Abbou, Mélanie Grignon

energies

MDPI

Article

Voltage Readjustment Methodology According to Pressure and Temperature Applied to a High Temperature PEM Fuel Cell †

Mathieu Baudy [1,*], Olivier Rondeau [2], Amine Jaafar [1], Christophe Turpin [1], Sofyane Abbou [2] and Mélanie Grignon [1]

[1] LAPLACE—Laboratoire Plasma et Conversion d'énergie Université de Toulouse, CNRS—Centre National de la Recherche Scientifique, Toulouse INP—Institut National Polytechnique de Toulouse, UPS—Université Paul Sabatier, F-31077 Toulouse, France; jaafar@laplace.univ-tlse.fr (A.J.); turpin@laplace.univ-tlse.fr (C.T.); grignon@laplace.univ-tlse.fr (M.G.)

[2] Safran Power Units, F-31019 Toulouse, France; olivier.rondeau@safrangroup.com (O.R.); sofyane.abbou@safrangroup.com (S.A.)

* Correspondence: mathieu.baudy@laplace.univ-tlse.fr

† This paper is an extended version of our paper published in IEEE International Conference on Electrical, Computer and Energy Technologies (ICECET 2021), Cape Town, South Africa, 9–10 December 2021; pp. 1–6.

Abstract: The operating conditions can have uncontrolled effects on the voltage of a High-Temperature Proton Exchange Membrane Fuel Cell (HT-PEMFC). For instance, the HT-PEMFC can be used at ambient pressure, i.e., without having a back pressure regulator. In this case, the variation in the atmospheric pressure directly affects pressures inside the fuel cell, which induces voltage variation. Moreover, in transient phases, several coupled phenomena can have an uncontrolled effect on the voltage. For example, following a change in the current operating point, thermal conditions in the fuel cell can vary, and the temperature stabilization then leads to a voltage variation. This article introduces a readjustment method for the fuel cell voltage to compensate for the effects of the pressure and temperature variations that are undergone and to decouple their effects. This methodology is based on the realization of a design of experiments to characterize the voltage sensitivity to pressure ([1; 1.5 bar]) and temperature ([120; 180 °C]) between 0.2 and 1 A/cm^2 of an Advent PBI MEA (formerly BASF Celtec®-P 1100 W). The data obtained allowed identifying an empirical model that takes into account the aging caused by the experiment. Finally, the methodology is criticized before proposing an alternative method.

Keywords: hydrogen; fuel cells; high temperature PEMFC; more electric aircraft; operating conditions; design of experiments; readjustment method; atmospheric pressure

Citation: Baudy, M.; Rondeau, O.; Jaafar, A.; Turpin, C.; Abbou, S.; Grignon, M. Voltage Readjustment Methodology According to Pressure and Temperature Applied to a High Temperature PEM Fuel Cell. *Energies* **2022**, *15*, 3031. https://doi.org/10.3390/en15093031

Academic Editor: Nicu Bizon

Received: 21 March 2022
Accepted: 15 April 2022
Published: 21 April 2022

1. Introduction

The total contribution of the aviation sector to global warming includes the effects of different phenomena such as direct emissions of CO_2 but also NO_x, water vapor, as well as the formation of condensation trails, soot aerosols and sulfate aerosols. The global warming potential calculation indicates that the aviation sector has an impact three times greater than the one retained by the single account of CO_2 effects [1]. Moreover, in 2018, 11% of the world's population flew at least once, and 1% made more than 50% of the flights [2]. In this context, the estimates published by the aircraft manufacturers Airbus and Boeing target an increase in the global fleet to more than 45,000 aircraft by 2038 [3,4]. A study carried out as part of the Clean Sky 2 and Fuel Cells and Hydrogen 2 projects proposed forecasts for the fleet composition that would make it possible to meet environmental challenges [5]. The scenarios consider the use of liquid hydrogen-powered propulsion by 2050 for 40–60% of the fleet [6]. It says that the use of fuel cells would allow a 75% to 90% reduction in climate impact compared to kerosene by canceling direct emissions and reducing the impact of

condensation trails [7]. In order to achieve these objectives, it is necessary to go through several development stages of a specific system before validating its use onboard.

It is in this development context of fuel cell technology that the PIPAA project ("PIle à combustible Pour Applications Aéronautiques") was created [8]. Piloted by Safran Power Units, the project aims to embark a fuel cell system in order to supply secondary loads on a business aircraft (for example, for cooking, entertainment or as an auxiliary power unit) [9,10]. In this case, the system must satisfy constraints related to both its mass and its size. The HT-PEMFC technology was developed in the 1990s and has several advantages that make it an interesting candidate for use in aircraft [11]. Indeed, its electrolyte composed of phosphoric acid (H_3PO_4) and a Polybenzimidazole (PBI) polymer allows its use between 120 and 180 °C. This gives it certain advantages for onboard use compared to other technologies. For example, compared to an LT-PEMFC (Low-Temperature Proton Exchange Membrane Fuel Cell) technology, the main advantages of an HT-PEMFC are:

- Better tolerance to CO, which permits, for example, an easier use with H_2 directly from hydrocarbon steam reforming (95% of the current world production) or biomethane [12–14];
- Use with dry gases (it is not necessary to use a gas humidification system when operating with air) [14,15];
- Simplified thermal management (easier cooling at higher ambient temperatures, which could be a real advantage for an aircraft on the airport tarmac in an arid zone).
- Moreover, compared to the LT-PEMFC, its main drawbacks are:
- Its longer start-up time (the fuel cell must be preheated to avoid the presence of liquid water harmful to the electrolyte) [13];
- The degradative secondary reactions are accelerated (catalyzed by the higher temperature) [13–15];
- The decrease in the kinetics of the oxygen reduction reaction (by H_3PO_4 adsorption on the electrode platinum catalyst) [16–19].

The operating conditions of an HT-PEMFC significantly impact the voltage. On the one hand, Rahim et al. studied the impact of operating conditions on performance using the design of experiments methodology as well as Rigal et al. [20,21]. They were particularly interested in the impact of temperature and stoichiometry. As in other studies, they reported their results at ambient pressure [22–26]. According to Waller et al., pressure has a significant impact on performance [27]. However, if the variation in the atmospheric pressure has a significant impact on the voltage, it could affect the analysis of the results.

The pressure stability of a fuel cell is sensitive to several factors. For example, we cite:

- Gas flow rates;
- Atmospheric pressure;
- Gas consumption by the H_2/O_2 redox reaction;
- External and internal leakage from the fuel cell.

Moreover, in a test where the fuel cell pressures would not be regulated, the atmospheric pressure variations over time affect the partial gases pressures within the electrodes and, therefore, the fuel cell voltage. In an example shown in Figure 1, the atmospheric pressure evolution (P_{atm1}) is presented. That leads to the evolution of the gas inlets ($P_{inA,anode1}$ and $P_{inA,cathode1}$). The voltage (U_{exp1}) decrease at around 300 h can then be immediately linked to the atmospheric pressure depression. Note that the pressure differences between the anode and the cathode are induced mainly by the differences in the flow rates that are applied. Indeed, the MEA manufacturer recommends maintaining constant stoichiometry in the functional current range (1.2 for H_2 at the anode and 2 for air at the cathode) and operating at ambient pressure. Thus, especially as the current increases, there is a difference that increases in favor of the inlet cathode pressure. As can be seen in Figure 2, this effect is also visible when making a polarization curve where the pressure of the gas outlet channels is not regulated. Note that the same effect would be seen if the back-pressure was regulated.

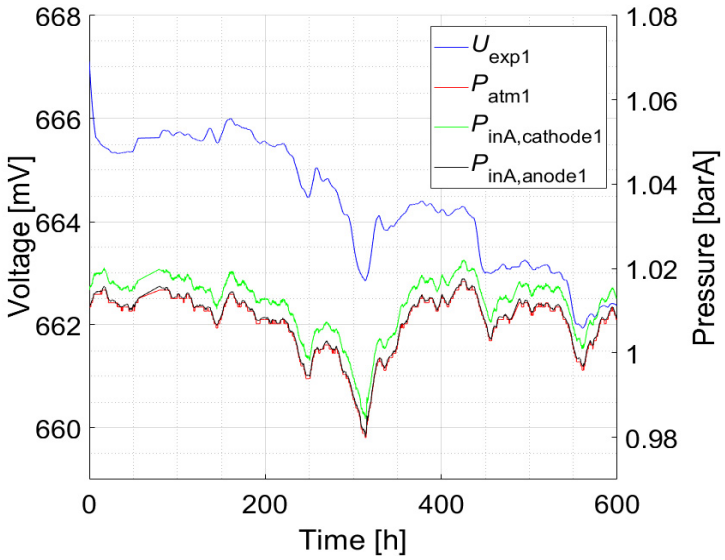

Figure 1. Temporal evolution of the voltage (U_{exp1}), H_2 ($P_{inA,anode1}$) and air ($P_{inA,cathode1}$) inlet pressures and atmospheric pressure (P_{atm1}) during a 600 h endurance test with an Advent PBI MEA (45.2 cm^2) operated at 160 °C, 0.2 A/cm^2, without back-pressure regulation and with stoichiometries of 1.2/2 for H_2/air.

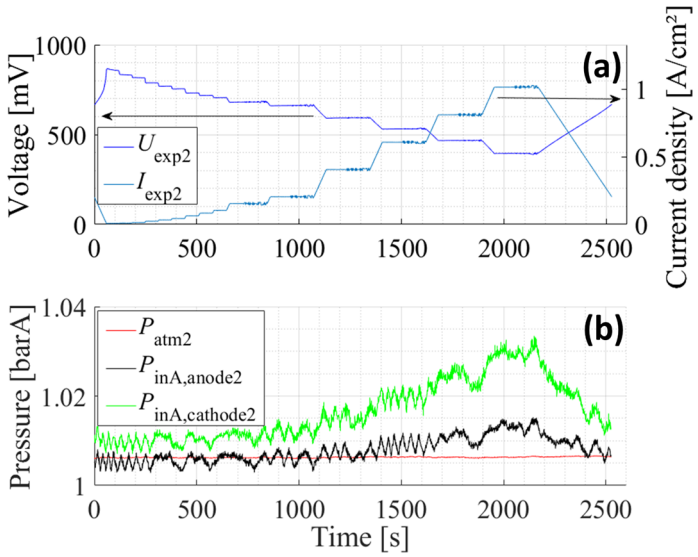

Figure 2. (**a**) Temporal evolution of the voltage (U_{exp2}) and current (I_{exp2}); (**b**) Corresponding H_2 ($P_{inA,anode2}$) and air ($P_{inA,cathode2}$) inlet pressures and atmospheric pressure (P_{atm2}). Recorded during a polarization curve of an Advent PBI MEA (45.2 cm^2) realized between 0 (open-circuit voltage) and 1 A/cm^2 at 160 °C, without back-pressure regulation and with stoichiometries of 1.2/2 for H_2/air.

On the other hand, the combination of effects related to several operating conditions in transient phases can also have an uncontrolled impact on the voltage. These can also influence the interpretation of the results. Zhang et al. highlighted these dynamics during the realization of the different steps of a polarization curve [28]. They explained them by a combination of effects related to the double-layer capacitance, the temperature variation, the reactants concentration and the conductivity of the membrane. These effects are simulated in the dynamic models that are realized to identify experimental data [29]. Moreover, other effects related, for example, to the oxidation of platinum can also have an impact [30,31]. However, the knowledge of the different time constants, sensitivities and mechanisms related to these phenomena can allow dissociating them.

The temperature stability of a fuel cell is sensitive to several factors. For example, we cite:

- Thermal inertia;
- Thermal control parameters of the test bench;
- Forced convection in the fuel cell channels;
- Operating point (more or less exothermal);
- External temperature and the fuel cell insulator.

Therefore, if a relatively fast current ramp is imposed on a fuel cell, the voltage changes until the current stabilizes. The different phenomena listed above then impact the temperature fuel cell. In turn, this leads to a variation in the voltage before reaching its stabilization point. This is what can be seen in Figure 3. Blue curves start at the end of a ramp from 1.0 to 0.2 A/cm^2 with a 3.3 mA/cm^2/s speed. Black curves start at the end of a ramp from 0 to 0.2 A/cm^2 with a 2.2 mA/cm^2/s speed. Only cathode temperatures are shown as anode temperatures behavior are similar (but signals are noisier). Note that the two acquisitions do not stop at the same time because they are from two different tests with two different stabilization times right after the ramps. Thus, both voltage variations driven by those of the current and the temperature are coupled during the current ramp. After the current stabilization, the voltage is only subject to the temperature variation until it stabilizes.

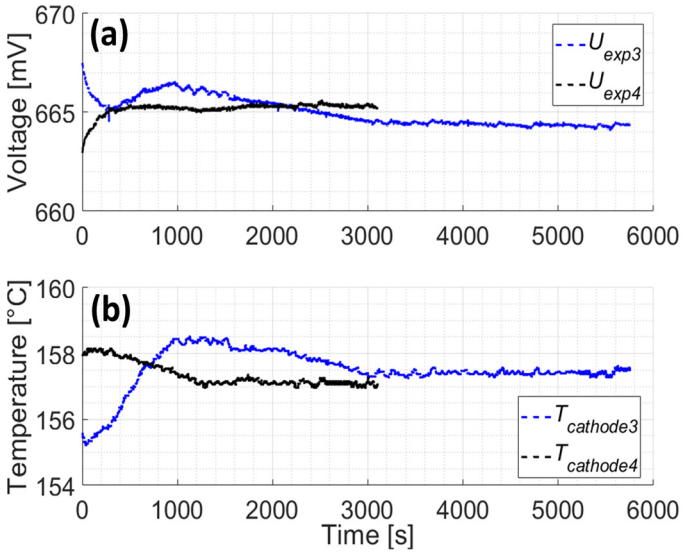

Figure 3. (**a**) Temporal evolution of voltages (U_{exp3}, U_{exp4}); (**b**) Corresponding cathode temperatures. Recorded at 0.2 A/cm^2 after two different ramps (not represented) using an Advent PBI MEA (45.2 cm^2), without back-pressure regulation and with stoichiometries of 1.2/2 for H_2/air.

The interest in knowing the sensitivity to the operating conditions of the fuel cell studied is, therefore, a requirement to ensure the correct interpretation of the test results. In cases where a comparison of data is necessary, it is then essential to take into account the impact of this sensitivity. For example, voltages on a polarization curve, recorded at the beginning and at the end of a test, which would not have been at the same atmospheric pressure (without back-pressure regulation), may not be directly comparable. Similarly, temperature differences induced by different dynamics affect the voltage and make the comparison difficult. In order to make these comparisons possible, a study was conducted to establish a methodology for readjusting the voltage to a single performance point chosen as a standard reference point. It should be used to readjust the temporal data for modeling purposes or simply for a better dynamics visualization.

In this article, a design of experiments is realized to characterize the pressure and temperature sensitivities of an HT-PEMFC MEA. The generated data are then modeled to

define voltage readjustment factors. Finally, examples and perspectives of use are proposed and discussed.

This article extends previous research [32] (preliminary results of this study were presented at the IEEE International Conference on Electrical, Computer and Energy Technologies (ICECET 2021)).

2. Experimentation

2.1. Material

First, a design of experiments was performed to characterize the impact of pressure and temperature on the performance of a commercial Advent PBI MEA manufactured by Advent Technologies, Patras, Greece. (formerly BASF Celtec®-P 1100 W, manufactured by BASF Fuel Cell GmbH, Ludwigshafen, Germany). The variation ranges of the different operating conditions were chosen to correspond to the MEA operating range. Only a restriction on the current range was made. Indeed, low current densities (<0.2 A/cm^2) are not explored because:

- They can degrade the MEA due to carbon corrosion which occurs significantly at high voltage (>0.8 V) [33,34];
- Voltage variations due to operating conditions at low currents are relatively smaller and therefore negligible;
- Positioning only on the voltage linear range can facilitate the identification of a linear model.

The MEA was manufactured in 2015 (vacuum packed for four years, active surface of 45.2 cm^2, thickness of 900 +/− 50 µm). It is installed in a BASF single cell test box, shown in Figure 4, constituted by:

- Two PFA gaskets (thickness: 345 +/− 5 µm);
- Two graphite gas flow plates (two 1 mm segmented serpentine channels at the anode and three 1 mm segmented serpentine channels at the cathode;
- Two electrical current collectors (copper);
- Two clamping plates with fluid interfaces (with Belleville washers; clamping of the test box at 3 N.m and fluidic interfaces in $\frac{1}{4}$" DB);
- Two heating elements (of 80 ohms supplied in series at 2 × 110 V).

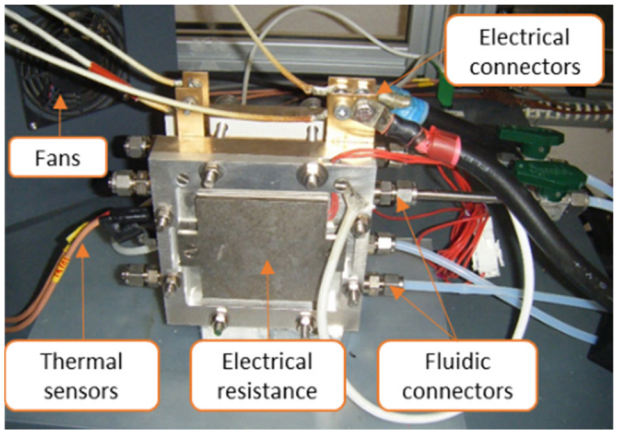

Figure 4. Photography of the HT-PEMFC test box in the in-house test bench.

Only the anode temperature is regulated using a thermocouple placed in the anode test box graphite plate. The test box is sealed by O-rings compressed between the clamping plates and the graphite plates on both sides of the box.

It is installed in a test bench consisting of the following components:

- An electronic load H&H PL306 (300/1000 W from 0 to 50 A);

- A Quality Source S402 power supply (5 V, 80 A, in series with the active load to allow its operation at low current);
- A discharge resistor (1 ohm, 1.3 W);
- A National Instrument (NI) DAQ-4461 board that drives the load via a NI-LabView interface performing electrochemical impedance spectrum analysis;
- The H_2, N_2 and air–fluid distribution equipment (filters, valves, flow regulators);
- Pressure sensors at the gas inlets of the fuel cell;
- Two phase separators by bubbling (the fuel cell gas outlets are slightly immersed in a volume of water to allow the recovery of phosphoric acid in case of electrolyte leakage);
- Micrometric valves at the gas outlets (manual back-pressure regulation).

The stoichiometries $\lambda_{H_2}/\lambda_{air}$ are maintained constant by the mass flow controllers at 1.2/2. Volume flow rates Q (in NL/min) as a function of the current density J (in A/cm^2) are given by Faraday's formula for H_2 (see (1)) and air (see (2)). The molar volume Vm is 22.41 L/mol at 0 °C and 1 atm. The Faraday constant F is 96485.33 C/mol. The proportion of O_2 in air x_{O_2} is taken to be 20.95%. Sa is the active area of the MEA (here, 45.2 cm^2).

$$Q_{H_2} = \lambda_{H_2} \cdot J \cdot Sa \cdot Vm/(2 \cdot F) \quad (1)$$

$$Q_{air} = \lambda_{air} \cdot J \cdot Sa \cdot 0.5 \cdot Vm/\left(2 \cdot F \cdot x_{O_2}\right) \quad (2)$$

2.2. Initial Test Phase and Characterizations

Once installed on the test bench, N_2 was introduced into both test box compartments at a flow rate of 0.2 NL/min while increasing the test box temperature to 160 °C. After checking the test box external leakage and the MEA internal leakage (between both compartments), the active gases were introduced, and the current density was increased to 0.2 A/cm^2. Then, the current was maintained for 72 h to perform the MEA break-in. The voltage increased during the break-in period from 670 mV to 695 mV. This increase could be attributed to an acid redistribution in the membrane [15].

The comparison of two current truncated polarization curves realized before and after the design of experiments in pressure and temperature shows a voltage decrease during the tests (see Figure 5). Both polarization curves were performed without back-pressure regulation. The initial polarization curve was recorded with an ambient pressure of 1.004 barA and the final polarization curve with 1.001 barA. Pressures are therefore not the same for each current step, as in Figure 2, as the stoichiometries are maintained constant. These polarization curves are therefore given as an indication. The voltage decreased by 1.6% at 0.2 A/cm^2 and by 6.7% at 1 A/cm^2. Thus, the test appears to have been degrading for the fuel cell. The test lasted 18 days (i.e., 384 h) between the initial and the final polarization curves. We can therefore calculate aging rates: −28 µV/h at 0.2 A/cm^2 and −75 µV/h at 1 A/cm^2. These aging rates are higher than those found in the literature [14,35–40], but they are similar to those of aging tests previously performed in the laboratory with similar material [24]. The observed degradation, therefore, appears to be caused by the different steps of the tests. Changes in temperature, pressure and current could have caused degradation in the MEA. An accumulation of reversible losses may also explain the observed voltage difference [19,23,29,30].

The evolution of the high-frequency resistance (R_{HF}) measured on the different current steps of the truncated polarization curves at the beginning and end of the tests was very low, as shown in Figure 6. This resistance was measured by performing Electrochemical Impedance Spectroscopy (EIS) on the current levels of the polarization curves. These EIS were performed from 20 kHz to 1 Hz with a peak-to-peak amplitude of 1 A. The high-frequency resistance corresponds to the value at which the imaginary part cancels at high frequencies after transformation in the complex plane of the voltage response with respect to the sinusoidal stress carried out in the current. Thus, the characterizations performed did not allow to make the hypothesis of a privileged degradation.

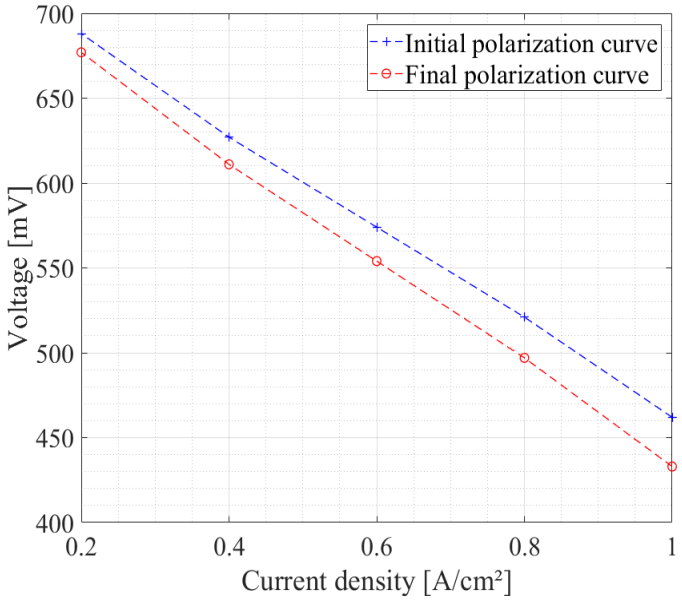

Figure 5. Truncated polarization curves before (initial) and after (final) the design of experiments in pressure and temperature between 0.2 and 1 A/cm^2 with stoichiometries of 1.2/2 for H_2/air, at 160 °C and at ambient pressure of 1.004 (initial) and 1.001 barA (final).

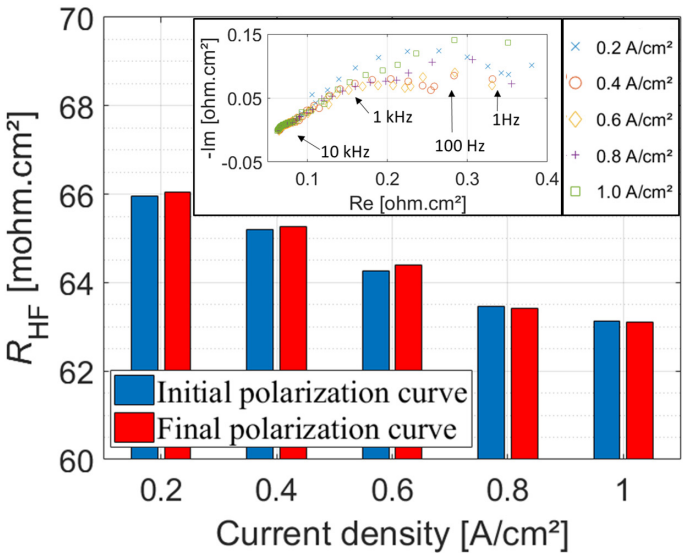

Figure 6. High-frequency resistances R_{HF} measured by EIS performed on the polarization curves before (initial) and after (final) the design of experiments in pressure and temperature represented in histograms as a function of the current density.

2.3. Design of Experiments in Pressure and Temperature

The acquisition of the different voltages was performed in the same order for each operating condition. First, the temperature was regulated to the desired value, the pressure was stabilized to be homogeneous in both compartments, and the different current points were tested. Adjustments must be made for each current to maintain the pressure at the desired value with both micrometric valves. The operating conditions' stabilization was verified before the data recording. Once the current range was fully explored, the pressure was changed to the next operating point value, and the current cycle was resumed from 0.2 A/cm^2. The return to the first pressure condition was performed to check the current and pressure variations impact the voltage before each temperature change. Moreover, a return to 160 °C enabled taking into account the impact of the entire test. Table 1 presents the

different operating conditions explored. Each condition was presented in the chronological order in which it was performed.

Table 1. The different operating conditions explored during the pressure and temperature design of experiments.

Temperature [°C]	[120; 160; 180; 140; 150; 155; 165; 170; 160]
Inlet pressure [barA]	[1; 1.1; 1.3; 1.5; 1]
Current Density [A/cm^2]	[0.2; 0.4; 0.6; 0.8; 1]

Note that it was not always possible to realize the points at 1 barA according to the value of the atmospheric pressure. In fact, part of the test for the same temperature was carried out on the same day. During this day, for each different pressure, the current was modified to reach the different corresponding values. Between two test days and during weekend days, the fuel cell was operated at 0.2 A/cm^2, 160 °C and at ambient pressure (the micrometric valves are fully open) with stoichiometries of 1.2/2 for H_2/air.

2.4. Results

Figure 7 shows the different voltages measured during the design of experiments as a current density function. We can see that there are more important differences at high currents while the pressure and the temperature change. Moreover, the cluster formed by these different voltages defines the single-cell current reduced functional domain. Both initial and final polarization curves previously presented in Figure 5 are displayed as well as the proposed reference curve for a BASF Celtec®-P 1100 W MEA (from the manufacturer) in order to validate their inclusion in the functional range.

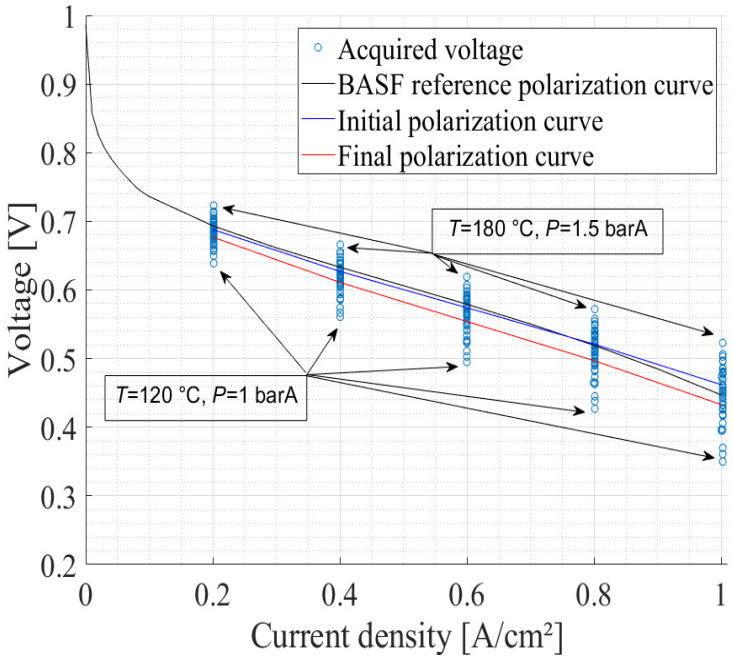

Figure 7. Representation of all the voltages measured during the design of experiments in pressure and temperature as a function of the current density. All series of data in pressure and temperature are not represented to lighten the graph. BASF, initial and final reference polarization curves from Figure 5 are reported.

Moreover, note that over the functional range studied, the cell voltage varies in the same direction as the pressure and the temperature. Additionally, the voltage variations

according to the current present a linear behavior with the pressure and the temperature, as can be observed in Figure 8.

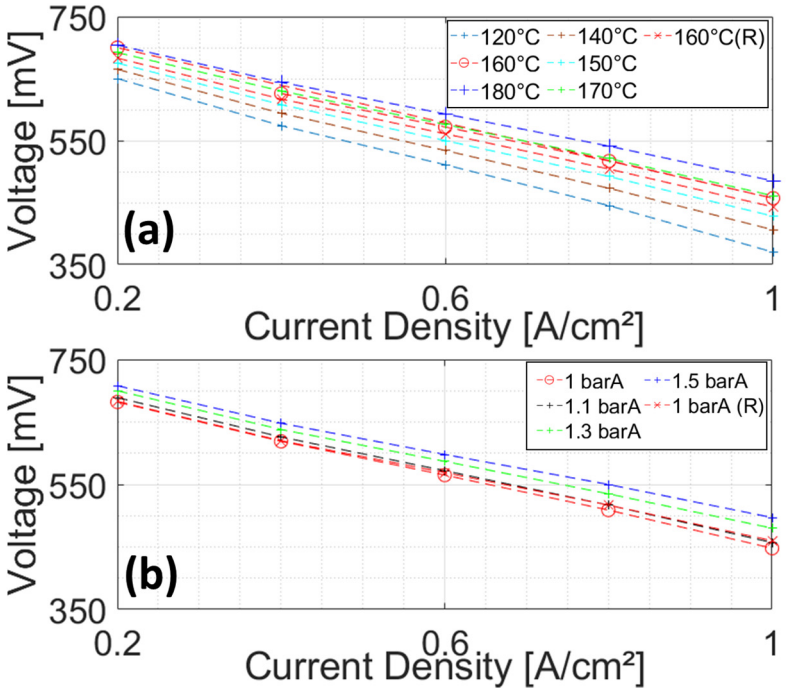

Figure 8. (**a**) Voltages as a function of current at 1.1 barA and for different temperatures (without 155 °C and 165 °C for clarity); (**b**) Voltages as a function of current density at 160 °C and for different pressures. (R) is annotated to indicate the return to the initial operating condition.

3. Development of the Readjustment Method

3.1. Definition of an Empirical Model Variables

An empirical model (see (3)–(6)) was proposed in order to study the predictive accuracy in the functional domain (restricted in current) of the single cell studied in the experiment. The objective of this modeling was to distinguish the contributions to the voltage, respectively, related to pressure and temperature. The parameters of pressure P, temperature T and aging h (the temporal parameter used to take into account the voltage degradation with the time) were declined by affine contributions according to the current density parameter J and coefficients $c_{i,j}$ with i and j used to identify to which parameter P, T, J and/or h they are related to. This model seems, at first sight, to be sufficiently complete in its cross consideration of the different parameters.

$$\begin{aligned} U_{\mathrm{Mod}}(J,P,T,h) = {} & Coef_P(J)\cdot P + Coef_T(J)\cdot T \\ & + Coef_h(J)\cdot h + c_J\cdot J \\ & + c_{\exp}\cdot \exp(J) + c_{\ln}\cdot \ln(J) \\ & + c \end{aligned} \tag{3}$$

$$Coef_P(J) = c_{P,J}\cdot J + c_P \tag{4}$$

$$Coef_T(J) = c_{T,J}\cdot J + c_T \tag{5}$$

$$Coef_h(J) = c_{h,J}\cdot J + c_h \tag{6}$$

In this model, the pressure P (in barA) is defined as the average pressure of the test box, calculated from the absolute inlet pressures of both anode ($P_{\mathrm{inA,anode}}$) and cathode ($P_{\mathrm{inA,cathode}}$) gas compartments according to (7).

$$P = (P_{\mathrm{inA,anode}} + P_{\mathrm{inA,cathode}}) \ / \ 2 \tag{7}$$

As the pressure is measured by the sensors relative to the atmospheric pressure, the inlet anode ($P_{\text{inG,anode}}$) and cathode ($P_{\text{inG,cathode}}$) gauge pressures can be introduced with the atmospheric pressure (P_{atm}) according to (8).

$$P = (P_{\text{inG,anode}} + P_{\text{inG,cathode}}) \ / \ 2 + P_{\text{atm}} \tag{8}$$

Similarly, the temperature T (in °C) is defined as the average temperature of test box, measured by the two thermocouples inserted in the anode (T_{anode}) and cathode (T_{cathode}) bipolar plates according to (9).

$$T = (T_{\text{anode}} + T_{\text{cathode}}) \ / \ 2 \tag{9}$$

3.2. Application to Data and Model Accuracy

Four different models were declined from U_{Mod} by putting some coefficients of (3)–(6) equal to zero. The other coefficients were obtained by performing linear regressions (see Table 2). The different proposed coefficients allowed the dissociation of the affine contributions linked to the different desired operating conditions independently of the ones linked to aging. Each model is therefore suitable for the development of the pressure $Coef_P$ (see (4)) and temperature $Coef_T$ (see (5)) coefficients.

Table 2. Values of the model coefficients used in Equations (3)–(6) and corresponding regress ion coefficients.

Param (Unit) \ Models		U_{Mod1}	U_{Mod2}	U_{Mod3}	U_{Mod4}
c_P	(mV/mbar)	3.82×10^{-2}	8.39×10^{-2}	8.03×10^{-2}	8.03×10^{-2}
c_T	(mV/°C)	7.14×10^{-4}	1.22×10^{-3}	1.48×10^{-3}	1.48×10^{-3}
c_h	(mV/h)	-9.22×10^{-6}	-2.70×10^{-5}	-2.12×10^{-5}	-2.12×10^{-5}
c_J	(mV/[A/cm^2])	-5.67×10^{-1}	-3.02×10^{1}	-3.24×10^{-1}	-2.66×10^{-1}
$c_{P,J}$	(mV/mbar/[A/cm^2])	7.07×10^{-2}	0	0	0
$c_{T,J}$	(mV/°C/[A/cm^2])	1.27	0	0	0
$c_{h,J}$	(mV/hour/[A/cm^2])	-1.95×10^{-2}	0	0	0
c_{ln}	(mV)	0	0	0	-1.28×10^{-2}
c_{exp}	(mV)	0	0	1.73×10^{-2}	0
c	(mV)	5.87×10^{2}	4.65×10^{-1}	4.08×10^{-1}	3.99×10^{-1}
Correlation coefficient r^2		9.97×10^{-3}	9.97×10^{-3}	9.92×10^{-3}	9.92×10^{-3}
Standard deviation σ		4.05×10^{-3}	2.76×10^{-3}	7.80×10^{-3}	7.75×10^{-3}

The first two empirical models, U_{Mod1} and U_{Mod2}, have similar r^2 regression coefficients (see Table 2) and are larger than the other two models. Moreover, the exponential (see U_{Mod3}) and logarithmic (see U_{Mod4}) contributions do not provide better accuracy compared to the U_{Mod2} model. In order to develop a readjustment method for pressure and temperature, it is the U_{Mod1} model that is retained. Indeed, although the U_{Mod2} model proposes a smaller standard deviation, U_{Mod1} allows dissociating affine contributions according to the current, linked to the desired operating conditions independently of those linked to aging. Moreover, the coefficients of the U_{Mod2} model would not allow taking into account that the sensitivities of the voltage to pressure and temperature are dependent on the current, as observed in Section 2.4. Therefore, it is more suitable for the development of readjustment factors (see (10)).

$$U_{\text{Mod1}}(J,P,T,h) = Coef_P(J)\cdot P + Coef_T(J)\cdot T + Coef_h(J)\cdot h + c_J\cdot J + c \tag{10}$$

Note that an improvement of the model in (10) was tried by adding a term with the variables P and T crossed. The newly generated coefficient only slightly improved the model accuracy while only slightly changing the other coefficients, so it was abandoned.

3.3. Generation of the Readjustment Factors

Therefore, the two affine equations corresponding to the pressure (see (4)) and to the temperature (see (5)) coefficients evolution according to the current density can be plotted (see Figure 9). Thus, if it is intended to readjust the voltage to the standard conditions (for example, T_{std} = 160 °C and P_{std} = 1 barA), corrections must be applied to the voltage value depending on the operating conditions (T ($\neq$160 °C) and P ($\neq$1 barA)). The experimental voltage U_{exp} of a cell (in mV), corrected in pressure P (in barA) and temperature T (in °C) was noted U_{Cor} (in mV), as shown in (11)–(13). Note that U_{Cor_T} and U_{Cor_P} are also defined in mV.

$$U_{\text{Cor}} = U_{\text{exp}} + U_{\text{Cor}_T} + U_{\text{Cor}_P} \tag{11}$$

$$U_{\text{Cor}_T} = Coef_T \cdot (T_{\text{std}} - T) \tag{12}$$

$$U_{\text{Cor}_P} = Coef_P \cdot (P_{\text{std}} - P) \cdot 10^3 \tag{13}$$

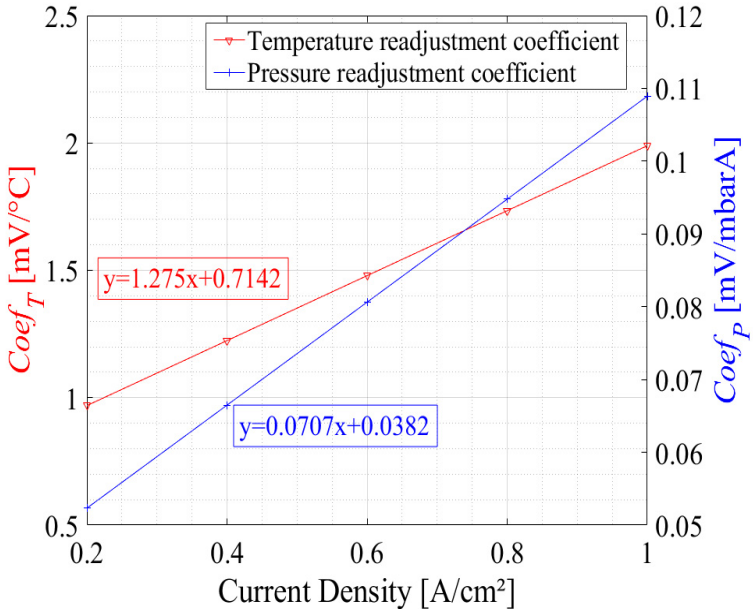

Figure 9. Generation of temperature (in red, see (5)) and pressure (in blue, see (4)) coefficients according to the current density and corresponding equations.

3.4. Application Examples

First, the readjustment methodology was applied to the test presented previously in Figure 1. Note that it used a similar test best bench and a similar test box to the one in Section 2. The aim is to readjust the voltage to the standard condition of P_{std} = 1 barA and T_{std} = 160 °C. The calculation of the average pressure P in the test box is first carried out according to (7) over the whole test duration. Then, the pressure coefficients given by (4) were used to calculate the readjustment factor U_{Cor_P} of (13). This term was then added to the voltage at each time t using (11). The result is drawn in Figure 10.

Moreover, the readjustment method is applied to the test previously presented in Figure 3. Note that it used a similar test box to the one presented in Section 2 while the test bench was the same. The application of the readjustment factors in temperature allows for smoothing the two curves, which allows for the visualization of a symmetrical dynamic (see Figure 11). It should be noted that for this example, the atmospheric pressure was also readjusted, which results in a variation of +1 mV on the whole green curve. Note that as the anode temperature was noisy, we observed the same noise on the corrected voltages. Thus, the readjustment methodology removed the effects of temperature dynamics on the voltage. The posterior modeling of both voltage dynamics thus allowed a comparison of

the current variation effects and also allowed decoupling the different stabilization times related to each operating condition.

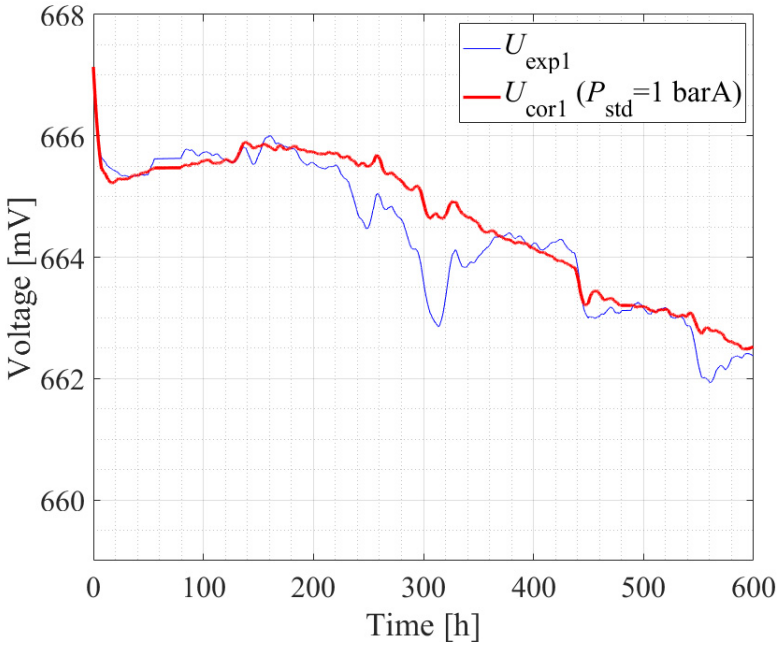

Figure 10. Application of the readjustment methodology for the pressure to the voltage from Figure 1. The corrected voltage U_{Cor1} is given at a standard pressure of 1 barA.

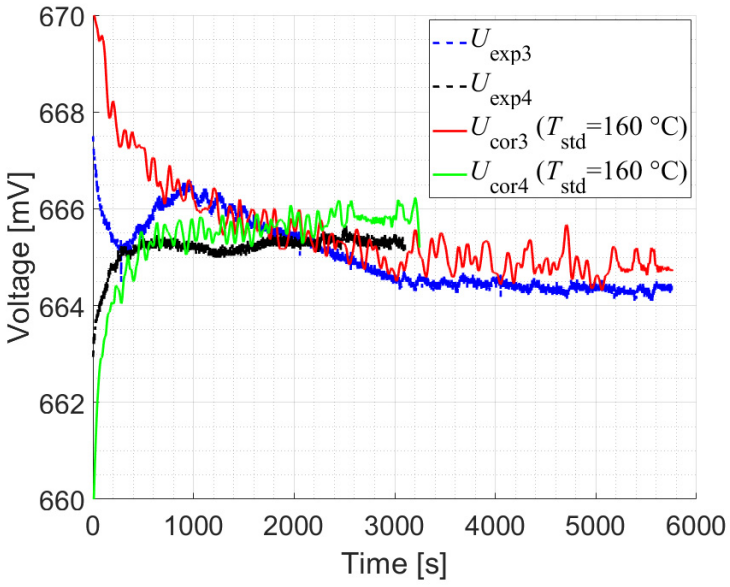

Figure 11. Application of the readjustment methodology for the temperature to the voltage from Figure 3. The corrected voltages U_{Cor3} and U_{Cor4} are given at a standard temperature of 160 °C.

4. Discussions and Perspectives

4.1. Critics and Limitations

Despite the short duration of the design of experiments in pressure and temperature (compared to aging tests more commonly carried out in a few hundred hours minimum) and despite the relative slowness of the current ramps between each point (in order to maintain the stability of the operating condition), a degradation is visible on the voltage between the beginning and the end of the experimentation. As this degradation cannot be explained by an increase in the high-frequency resistance (see Section 2.2), other phenomena

are certainly at stake. The limitation of the functional domain in current also seems to make it possible not to consider the hypothesis of carbon corrosion. Other characterizations, such as post-mortem microscopic analysis, could provide further insight. Thus, whether irreversible or reversible, the observed voltage losses are strongly related to how the test was performed. However, the empirical model was identified by taking into account the specific aging of this test. It cannot be excluded that the sensitivity of the voltage to the operating conditions can be different according to the degradation. Therefore, the model is not necessarily valid if the fuel cell is exposed to other types of degradation.

Moreover, the test bench used to generate the coefficients can be a source of limitation in applying the methodology to data from other test benches. Indeed, the gas pipes can be of different dimensions or with other fluidic equipment, especially at the gas outlets. This would generate different pressure drops, which would then have an impact on the pressure gradient in the fuel cell. As the pressures were only measured at the fuel cell inlets and not at the outlets, it is not possible from the data collected to extrapolate a model for an average pressure of each fuel cell compartment (which would therefore be applicable for the test box, whatever the test bench).

Note that the use of micrometric valves adds pressure drops between the fuel cell gas outlet and the atmospheric pressure. Nevertheless, when these valves and the gas outlet pipes were dismantled after the test, no condensed phosphoric acid was found. Therefore, it does not seem that the test resulted in any particular condensation of the acid as it was not found in the bubble water either. Thus, there would be no objection to the use of fuel cell outlet pressure sensors for this type of test.

It is also important to note that pressure differences between the anode and cathode are not taken into account when applying the methodology. Indeed, as in the example of the polarization curve visible in Figure 2, if there is no pressure regulation, both compartments will have different pressures over a large part of the functional range (depending on the atmospheric pressure). In order to establish a more accurate quantitative calibration, it would be necessary to realize a design of experiments on the average pressure of each compartment (with pressure sensors at the gas outlet), which would take into account the differences between anode and cathode. For example, the design of experiments will consider a variation in the outlet pressures and record the inlet pressures and resulting voltage. It is then possible to propose modeling according to the average pressures of each compartment.

Additionally, this observation can also be extended to the use of a different test box. In the proposed application on the pressure (see Section 3.4), the test is performed with a test box installed on a different test bench but with the same type of MEA as used in the experimental design in this article. Let us note, however, that they are not from the same manufacturing batch. The results seem to be qualitatively coherent after the readjustment. However, it is difficult to validate quantitatively that the applied coefficients are the most appropriate.

Furthermore, in the case of pressure, a technical difficulty may lead to extrapolating the model outside the domain in which it was built. Indeed, in the design of experiments, the pressure points must necessarily be higher than the atmospheric pressure to be realized with the material proposed in Section 2. Thus, if we wish to readjust a voltage that was taken at a pressure below the minimum explored during the design of experiments, we must necessarily extrapolate the model. In order to achieve pressure points lower than atmospheric pressure in the design of experiments, one possibility would be to use gas pumping equipment at the outlets to decrease the pressure after the micrometer valves. It would then also be necessary to change the size of the micrometric valves or to use, for example, adapted proportional valves.

Finally, the extrapolation of the readjustment coefficients to the use of stacks (using the same MEAs) does not seem directly applicable and would require further work. Nevertheless, the method seems all the more interesting to apply because of the greater impact of the operating conditions on the voltage due to the multiplication of the number of cells.

4.2. Reduced Design of Experiments at the Beginning and End of a Test

During each test consisting of aging an MEA, an initial and a final characterization phase are commonly performed. Each phase may include, for example, polarization curve, electrochemical impedance spectroscopies or even cyclic voltammetry [21]. In the cases where it seems necessary to define readjustment coefficients, the realization of a targeted design of experiments seems relevant. This would assume linearity of the voltage responses as a function of pressure and temperature over the range where the voltage varies linearly (in the middle of the polarization curve).

These assumptions, already verified for the fuel cell used in Section 2 of this article, allow limiting the number of performance points to be realized in order to deduce usable readjusting coefficients. By also knowing the stabilization dynamics of the different controllers and the fuel cell, adequate stabilization times can be defined between each performance point. Thus, considering the linearity hypothesis, two pressure and temperature points can be chosen around the standard conditions for which the readjustment is desired. These performance points must be consistent with the functional domain in which the fuel cell evolves during the test. For example, in the context of an aging test left at atmospheric pressure, it seems appropriate to use two pressure points as 1.00 and 1.05 barA. Note that it would be interesting to measure the gas test box outlets' pressures in order to consider the average pressures of each compartment and so, to simulate the variation in the atmospheric pressure as if it were directed at the test box outlet. Thus, there would be eight performance points to achieve. In this example, they could be those proposed in Table 3. Given the few points, the small gradients and the time to realize it (1 h approximately), the assumed hypothesis is that it should not generate degradations.

Table 3. The different operating conditions explored during the reduced pressure and temperature design of experiments.

Temperature [°C]	[160; 165]
Outlet pressure [barA]	[1.00; 1.05]
Current Density [A/cm^2]	[0.2; 0.8]

In order to generate the readjustment coefficients, the coefficients in (10) must be identified using the experimental data set. The pressure coefficients are then given by (4) and the temperature coefficients by (5). Finally, to readjust to desired standard conditions of T_{std} and P_{std}, it is necessary to use (11)–(13).

It is proposed to repeat this design of experiments with the same points at the end of the test in order to quantify the impact of aging on the sensitivity of the voltage to the operating conditions. Thus, it is possible to compare the sensitivity of the voltage to pressure and temperature between the beginning and the end of the test. If there is a change in sensitivity, it will then be interesting to investigate the origin of this difference. This comparison could also help to understand the potential degradation caused by the test.

If the objective is to define coefficients that can be used for the same MEA regardless of the tests, the test boxes or the test benches used, then a perspective would be to compare the different coefficients generated between different tests. Furthermore, this would allow comparing the impact of specific degradations caused by the test on the voltage sensitivity to the operating conditions. For this purpose, the performance points of the design of experiments should be performed in the same way.

5. Conclusions

This article introduces a readjustment method for the HT-PEMFC voltage according to pressure and temperature. The objective is to compensate for the effects of the variations in the operating conditions that are undergone and to decouple their effects. An empirical model of an Advent PBI MEA is defined from the experimental data of a design of experiments performed on a truncated current domain between 0.2 and 1 A/cm^2. The design of

the experiments was degrading: −28 µV/h at 0.2 A/cm^2 and −75 µV/h at 1 A/cm^2 (for 384 h). The consideration of aging by linear approximation over time allowed identifying two independent equations that express the sensitivity of the voltage to temperature and pressure. They are estimated to 1 mV for 1 °C and 0.5 mV for 10 mbar at 0.2 A/cm^2 and to 2 mV for 1 °C and 1 mV for 10 mbar at 1 A/cm^2.

The application of this method allowed the fuel cell voltage to be readjusted on a test where atmospheric pressure caused different voltage variations over time. The readjustment permitted to limit the number of time domains where the voltage varies linearly. The second example in which the method was applied and verified resulted in the readjustment of the voltage during a transient phase where the temperature variation generated a voltage oscillation. The readjustment allowed finding a transient with a logarithmic behavior. Thus, it is possible thereafter to realize a finer identification of the physico-chemical phenomena that led to these various variations without bias caused by the variations in the operating conditions. The main limitation that was identified for the application of this method is that it does not allow to take into account if degradation has impacted these sensitivities.

Author Contributions: Conceptualization, M.B. and O.R.; methodology, O.R.; software, O.R.; validation, M.B.; investigation, M.G.; writing—original draft preparation, M.B.; writing—review and editing, A.J. and S.A.; supervision, C.T. All authors have read and agreed to the published version of the manuscript.

Funding: The authors would like to thank Safran Power Units and the Banque Publique d'Investissement (Bpifrance) for the financing of this work.

Data Availability Statement: The data that support the findings of this study are available on request from the corresponding author M.B.

Acknowledgments: The authors would like to express their sincere thanks to all the members of the PIPAA project and to all the public funders (FEDER, Occitanie Region, French Government, and Toulouse Metropole) of the LAPLACE Hydrogen Platform used for all tests during the PIPAA project.

Conflicts of Interest: The authors declare no conflict of interest. The funders had no role in the design of the study; in the collection, analyses, or interpretation of data; in the writing of the manuscript, or in the decision to publish the results.

References

1. Lee, D.S.; Fahey, D.W.; Skowron, A.; Allen, M.R.; Burkhardt, U.; Chen, Q.; Doherty, S.J.; Freeman, S.; Forster, P.M.; Fuglestvedt, J.; et al. The contribution of global aviation to anthropogenic climate forcing for 2000 to 2018. *Atmos. Environ.* **2021**, *244*, 117834. [CrossRef]
2. Gössling, S.; Humpe, A. The global scale, distribution and growth of aviation: Implications for climate change. *Glob. Environ. Change* **2020**, *65*, 102194. [CrossRef]
3. Global Market Forecast | Airbus. Available online: https://www.airbus.com/en/products-services/commercial-aircraft/market/global-market-forecast (accessed on 15 March 2022).
4. Boeing: Commercial Market Outlook. Available online: https://www.boeing.com/commercial/market/commercial-market-outlook/ (accessed on 15 March 2022).
5. Hydrogen-Powered Aviation. Available online: https://www.fch.europa.eu/publications/hydrogen-powered-aviation (accessed on 14 September 2021).
6. Winnefeld, C.; Kadyk, T.; Bensmann, B.; Krewer, U.; Hanke-Rauschenbach, R. Modelling and designing cryogenic hydrogen tanks for future aircraft applications. *Energies* **2018**, *11*, 105. [CrossRef]
7. Gierens, K. Theory of contrail formation for fuel cells. *Aerospace* **2021**, *8*, 164. [CrossRef]
8. Le Projet Collaboratif PIPAA, Piloté par Safran, Bénéficie D'une aide de 19,3 Millions D'euros Dans le Cadre du Programme d'Investissements d'Avenir (PIA) opéré par Bpifrance. Available online: https://www.safran-group.com/fr/espace-presse/projet-collaboratif-pipaa-pilote-safran-beneficie-dune-aide-193-millions-deuros-cadre-du-programme-2017-11-20 (accessed on 15 March 2022).
9. Report of the DOE-DOE Workshop on Fuel Cells in Aviation: Workshop Summary and Action Plan | Department of Energy. Available online: https://www.energy.gov/eere/fuelcells/downloads/report-doe-doe-workshop-fuel-cells-aviation-workshop-summary-and-action (accessed on 15 March 2022).
10. Friedrich, K.A.; Kallo, J.; Schirmer, J.; Schmitthals, G. Fuel cell systems for aircraft application. *ECS Trans.* **2009**, *25*, 193. [CrossRef]

11. Hooshyari, K.; Amini Horri, B.; Abdoli, H.; Fallah Vostakola, M.; Kakavand, P.; Salarizadeh, P. A review of recent developments and advanced applications of high-temperature polymer electrolyte membranes for PEM fuel cells. *Energies* **2021**, *14*, 5440. [CrossRef]
12. Vang, J.R. *HTPEM Fuel Cell Impedance: Mechanistic Modelling and Experimental Characterisation*; Department of Energy Technology, Aalborg University: Aalborg, Denmark, 2014; ISBN 978-87-92846-47-1.
13. Chandan, A.; Hattenberger, M.; El-kharouf, A.; Du, S.; Dhir, A.; Self, V.; Pollet, B.G.; Ingram, A.; Bujalski, W. High temperature (HT) polymer electrolyte membrane fuel cells (PEMFC)—A review. *J. Power Sources* **2013**, *231*, 264–278. [CrossRef]
14. Schmidt, T.J.; Baurmeister, J. Properties of high-temperature PEFC Celtec®-P 1000 MEAs in start/stop operation mode. *J. Power Sources* **2008**, *176*, 428–434. [CrossRef]
15. Schmidt, T.J. High-temperature polymer electrolyte fuel cells: Durability insights. In *Polymer Electrolyte Fuel Cell Durability*; Büchi, F.N., Inaba, M., Schmidt, T.J., Eds.; Springer: New York, NY, USA, 2009; pp. 199–221. ISBN 978-0-387-85536-3.
16. Authayanun, S.; Im-orb, K.; Arpornwichanop, A. A review of the development of high temperature proton exchange membrane fuel cells. *Chin. J. Catal.* **2015**, *36*, 473–483. [CrossRef]
17. Scott, K.; Pilditch, S.; Mamlouk, M. Modelling and experimental validation of a high temperature polymer electrolyte fuel cell. *J Appl Electrochem* **2007**, *37*, 1245–1259. [CrossRef]
18. Sood, R. Electrolytes Polymère Nano-Structurés à Base de Liquides Ioniques Pour les Piles à Combustible Hautes Températures. Ph.D. Thesis, Université de Grenoble, Grenoble, France, 2012.
19. Kaserer, S.; Caldwell, K.M.; Ramaker, D.E.; Roth, C. Analyzing the Influence of H3PO4 as catalyst poison in high temperature PEM fuel cells using in-operando X-ray absorption spectroscopy. *J. Phys. Chem. C* **2013**, *117*, 6210–6217. [CrossRef]
20. Rahim, Y.; Janßen, H.; Lehnert, W. Characterizing membrane electrode assemblies for high temperature polymer electrolyte membrane fuel cells using design of experiments. *Int. J. Hydrog. Energy* **2017**, *42*, 1189–1202. [CrossRef]
21. Rigal, S.; Turpin, C.; Jaafar, A.; Chadourne, N.; Hordé, T.; Jollys, J.-B. Steady-state modelling of a HT-PEMFC under various operating conditions. In Proceedings of the 2019 IEEE 12th International Symposium on Diagnostics for Electrical Machines, Power Electronics and Drives (SDEMPED), Toulouse, France, 27–30 August 2019; pp. 439–445.
22. Liu, S.; Rasinski, M.; Rahim, Y.; Zhang, S.; Wippermann, K.; Reimer, U.; Lehnert, W. Influence of operating conditions on the degradation mechanism in high-temperature polymer electrolyte fuel cells. *J. Power Sources* **2019**, *439*, 227090. [CrossRef]
23. Yezerska, K.; Liu, F.; Dushina, A.; Sergeev, O.; Wagner, P.; Dyck, A.; Wark, M. Analysis of the regeneration behavior of high temperature polymer electrolyte membrane fuel cells after hydrogen starvation. *J. Power Sources* **2020**, *449*, 227562. [CrossRef]
24. Rigal, S.; Turpin, C.; Jaafar, A.; Hordé, T.; Jollys, J.-B.; Chadourne, N. Ageing tests at constant currents and associated modeling of high temperature PEMFC MEAs. *Fuel Cells* **2020**, *20*, 272–284. [CrossRef]
25. Rastedt, M.; Pinar, F.J.; Pilinski, N.; Dyck, A.; Wagner, P. Effect of operation strategies on phosphoric acid loss in HT-PEM Fuel Cells. *ECS Trans.* **2016**, *75*, 455–469. [CrossRef]
26. Tingelöf, T.; Ihonen, J.K. A rapid break-in procedure for PBI fuel cells. *Int. J. Hydrog. Energy* **2009**, *34*, 6452–6456. [CrossRef]
27. Waller, M.G.; Walluk, M.R.; Trabold, T.A. Performance of high temperature PEM fuel cell materials. Part 1: Effects of temperature, pressure and anode dilution. *Int. J. Hydrog. Energy* **2016**, *41*, 2944–2954. [CrossRef]
28. Zhang, C.; Liu, Z.; Zhou, W.; Chan, S.H.; Wang, Y. Dynamic performance of a high-temperature PEM fuel cell—An experimental study. *Energy* **2015**, *90*, 1949–1955. [CrossRef]
29. Abdul Rasheed, R.K.; Liao, Q.; Caizhi, Z.; Chan, S.H. A review on modelling of high temperature proton exchange membrane fuel cells (HT-PEMFCs). *Int. J. Hydrog. Energy* **2017**, *42*, 3142–3165. [CrossRef]
30. Prokop, M.; Bystron, T.; Belsky, P.; Tucek, O.; Kodym, R.; Paidar, M.; Bouzek, K. Degradation kinetics of Pt during high-temperature PEM fuel cell operation part III: Voltage-dependent Pt degradation rate in single-cell experiments. *Electrochim. Acta* **2020**, *363*, 137165. [CrossRef]
31. Kregar, A.; Tavčar, G.; Kravos, A.; Katrašnik, T. Predictive virtual modelling framework for performance and platinum degradation modelling of high temperature PEM fuel cells. *Energy Procedia* **2019**, *158*, 1817–1822. [CrossRef]
32. Baudy, M.; Rondeau, O.; Jaafar, A.; Turpin, C.; Abbou, S.; Grignon, M.; Escande, A.; Rigal, S. Methodology for readjusting the voltage according to the operating conditions of a high temperature proton exchange membrane fuel cell. In Proceedings of the 2021 International Conference on Electrical, Computer and Energy Technologies (ICECET), Cape Town, South Africa, 9–10 December 2021. [CrossRef]
33. Mench, M.M. *Fuel Cell Engines*; John Wiley & Sons, Inc.: Hoboken, NJ, USA, 2008; p. 409.
34. Qi, Z.; Buelte, S. Effect of open circuit voltage on performance and degradation of high temperature PBI–H_3PO_4 fuel cells. *J. Power Sources* **2006**, *161*, 1126–1132. [CrossRef]
35. Modestov, A.D.; Tarasevich, M.R.; Filimonov, V.Y.; Zagudaeva, N.M. Degradation of High Temperature MEA with PBI-H3PO4 Membrane in a Life Test. *Electrochim. Acta* **2009**, *54*, 7121–7127. [CrossRef]
36. Oono, Y.; Sounai, A.; Hori, M. Influence of the phosphoric acid-doping level in a polybenzimidazole membrane on the cell performance of high-temperature proton exchange membrane fuel cells. *J. Power Sources* **2009**, *189*, 943–949. [CrossRef]
37. Li, Q.; Aili, D.; Hjuler, H.A.; Jensen, J.O. *High Temperature Polymer Electrolyte Membrane Fuel Cells: Approaches, Status, and Perspectives*; Springer: Cham, Switzerland, 2016; ISBN 978-3-319-17082-4.
38. Galbiati, S.; Baricci, A.; Casalegno, A.; Marchesi, R. Degradation in phosphoric acid doped polymer fuel cells: A 6000 h parametric investigation. *Int. J. Hydrog. Energy* **2013**, *38*, 6469–6480. [CrossRef]

39. Søndergaard, T.; Cleemann, L.N.; Becker, H.; Steenberg, T.; Hjuler, H.A.; Seerup, L.; Li, Q.; Jensen, J.O. Long-term durability of PBI-based HT-PEM fuel cells: Effect of operating parameters. *J. Electrochem. Soc.* **2018**, *165*, F3053–F3062. [CrossRef]
40. Büsselmann, J.; Rastedt, M.; Klicpera, T.; Reinwald, K.; Schmies, H.; Dyck, A.; Wagner, P. Analysis of HT-PEM MEAs' long-term stabilities. *Energies* **2020**, *13*, 567. [CrossRef]